Elsevier Editorial(tm) for Advances in Space Research
Manuscript Draft

Manuscript Number:

Title: An Atlas of Solar Events : 1997-2004

D2.5/E3.5-0004-04

Article Type: Contributed Paper

Keywords: Keywords
Solar events; Coronal mass ejections; dimmings; temperature effects; chromosphere
≈

Corresponding Author: Dr Guy Artzner CNRS

Other Authors: Artzner Guy, Dr; Auchère Frédéric, Dr; Delaboudinière Jean-Pierre, Dr; Bougnet Marie IAS-CNRS, IAS, IAS-CNRS, IAS CNRS

An Atlas of Solar Events : 1997-2004

G. Artzner, F. Auchère, J.P. Delaboudinière, M. Bougnet

Institut d'Astrophysique Spatiale, CNRS UMR 8617, bâtiment 121, Université Paris Sud, 91405 Orsay Cedex, France
guy.artzner@ias.u-psud.fr

Abstract

Coronal mass ejections (CMEs) are observed in the plane of the sky from coronographic images. As the solar surface is then masked by an occulting disk, it is not clear wether halo CMEs are directed towards the Earth or in the opposite direction. Observations of the solar corona on the solar disk from the Extreme Ultraviolet Imaging Telescope EIT on board the Solar Heliospheric Observatory SoHO do help in order to make a choice.

Quasi-continuous observations of the corona of the Sun have been therefore obtained from april 1997 up to now at a twelve minute cadence in the coronal line of FeXII, as a "CME watch program". At a slower six hours cadence an additional synoptic program investigates the chromosphere and the corona at four different wavelengths.

Large coronal solar events appear when viewing animations of the CME watch program. Fainter events do appear when viewing running difference animations of the CME watch program. When looking for additional spectral information from raw running differences of the synoptic program it is difficult to disentangle intrinsic solar events from the parasitic effect of the solar rotation. We constructed from the synoptic program observations an atlas of more than 30 000 difference images corrected for an average solar rotation.

We present case studies of specific events in order to investigate the source of darkenings or dimmings in difference images, either removal of emitting material, interposition of obscuring matériel, large changes of temperature or Doppler dimming.

As a by-product of the atlas of solar events we obtain a number of quiet time sequences well suited in order to precisely measure the differential solar rotation by the apparent displacement of tracers.

Testing an hypothesis is another (potential) by-product: the solar corona is heated by some interaction of galactic dark matter with solar magnetic fields.

1 Introduction

1-1 High cadence observations

Accretion or avulsion are common features of the evolution of most astrophysical objects. The detachment of matter from a celestial body is most precisely observed on the Sun when

coronographs detect coronal mass ejections (CMEs) as bright structures moving away from the sun in the plane of the sky. As the surface of the solar disk is then masked by the occulting disk of the coronograph it is difficult to determine whether the direction of a CME along the observing line, is directed towards Earth or in the opposite direction. In the catalog, http://cdaw.gsfc.nasa.gov/CME_list/, of CMEs observed since January 1996 with SoHO's coronographs, Brueckner et al., 1995, solar disk animations from the Extreme ultraviolet Imaging Telescope, EIT, Delaboudinière et al., 1995, appear in addition to coronographic data . An examination of this catalog reveals that the cadence for the disk data is slow, not better than a few images per day, until December 1996, when it became clear that at higher cadence, a few images per hour, sifting Earth directed CMEs became possible when coronal activity is simultaneously observed on the disk with the EIT imager on board SoHO, Domingo et al., (1995). This is the "CME watch program"

Due to the limited telemetry rate from the spacecraft it can be argued that a best compromise between temporal and spatial resolution is obtained when the displacement of observed waves from one image to the next amounts to a few pixels. This sampling criterion is not satisfied for EIT. However at a still too slow cadence of a few images per hour large solar events appear immediately when viewing an animation of instantaneous images and smaller events appear as easily from an animation of running difference images, as demonstrated by more than forty publications from the CME watch program listed in ftp://ftp.ias.u-psud.fr/pub/gartzner/GEA/biblio_differences-EIT.htm.

1-2 Slow cadence observations

In addition to the choice between spatial and temporal resolution, the observing modes of EIT offer a choice of four observing wavelengths defined by a filter wheel. The four wavelengths are centered around solar emission lines: three coronal lines of FeIX-FEX, FeXII and FeXIV around respectively 171Å, 195Å and 284Å and a 304Å channel for a blend of the 304Å HeII chromospheric line and of the 303.3Å SiXI coronal line. Again, due to the limited telemetry rate and to limitations from the filter wheel mechanism, the use of the spectral potentialities of EIT is usually restricted to a synoptic program of four quadruplets of 1024x1024 2"6 x 2"6 pixels images per day, at a six hours cadence starting at 01UT.

As the time scale of solar events is usually shorter than the six hours cadence of the synoptic program, extracting some spectral information from the images of this synoptic program is possible for large isolated solar events located shortly before 01UT, 07UT, 13UT or 19UT. If the amplitude of intensity variations induced by the event is small it is advisable to examine a

difference. In this case, in addition to the intrinsic time sampling problem, another difficulty arises: directly computing the difference of two images mainly displays the east-west gradient of the current image. Taking into account solar rotation removes this inconvenience.
We indicate in section 2 how we constructed an atlas of more than 8200 quadruplets of synoptic differences from april 1996 to September 2003. Subection 2-3 elaborates about the sensitivity of the solar events detection scheme. The results of the examination of ten solar events around various solar structures is given in section 3.

2 Technique

2.1 Computing an atlas of differences

EIT raw images present grid artefacts. As the grid artefacts are parallel to the spacecraft axis, i.e. usually parallel to the solar equator, rotation-corrected difference images from raw data present artefacts as north-south stripes, as noted by Chertok and Grechnev (2003). In order to remove these artefacts we used calibrated images taking into account the fact that the grid effects are clearly channel dependent. In the same line of reasoning we noted that difference computed from roll affected images display a slight residual grid effect at some angle to the direction of the solar equator.
Removing grid artefacts helps in order to detect faint solar events. A second effect has to be considered as described below. We suppose that the solar structures are immutable and that the instrumental effects are completely removed. We also suppose that the amplitude of solar rotation is so small that the variation of emissivity with angle is negligible. As a result, the difference of two images corrected for solar rotation should have a zero mean value. However the local value of the difference depends upon the statistical noise in such a way that the difference still somehow reflects the solar structures, instead of displaying a uniform value as expected. In order to obtain a better sensitivity for detecting time variations between images we divided the value of the difference by a quantity proportional to the expected statistical noise of this difference.
When due to the loss of data the time difference becomes larger than six hours, i.e. twelve or eighteen hours, the variation of emissivity with angle is no longer negligible, especially close to the limb. We noted systematic darkenings or brightenings close respectively to the east and west limb, as explained by par Sterling and Moore, 2004.

2.2 Reading an atlas of differences

Our atlas of synoptic differences does not include the larger set of data from the CME watch program. However the CME catalog allows a thorough and easy access to animations of CME

related images, graphs of linear and parabolic velocity fits and tabular data, including animations from EIT's CME watch program, the time when a CME enters in the C2 field of view and the extrapolated time back to the solar surface. It should be noted that during the few times when SoHO X axis is not parallel to the solar equator, i.e. when the value of the roll angle is different from zero, animations are presented uncorrected whereas the indicated tabular values of position angle for CMEs are roll corrected.

A six hours sampling interval is clearly too wide in order to investigate easily solar events. Taking partially into account aliasing effects is accomplished as described below. Successive differences are alternatively displayed in the right and left part of a screen. This allows to check in the previous difference the location of any brightening or dimming appearing in the current difference, in order to eliminate "ghost" dimmings due to an isolated brightening. This is the reason why figures 1 to 14 present several successive differences.

In the preceding subsection we elaborate on two points pertaining to the sensitivity of detection of solar events, removing grid artefacts and taking into account the effect of statistical noise. A third point to be considered is the fact that the dynamic of the images is greater than the dynamic of displays. This implies that examining a difference image from a display reveals time variations fainter than could be detected by the comparative examination of two successive instantaneous images.

According to the legends of figures 1 to 14 the time simultaneity of the four spectral bands of the synoptic observations is not perfect.

2-3 sensitivity of the solar events detection scheme

In this subsection we present a sample of four solar events of decreasing magnitude. *Italic script* numbers pertain to the number in our catalog of synoptic differences for the first difference image in the current figure.

The last row of figure 1 clearly displays intense brightenings and dimmings. They are less comfortably detected when viewing differences uncorrected for solar rotation or instantaneous images. The CME catalog indicates seven CMEs during the time span of figure 1, including a halo CME entering the field of view of the C2 coronograph at 15:26. We estimate with quasi certainty that the main structures in the third row of figure 1, 19UT-13UT differences, are related to this halo CME.

The darkening and the brightening of figure 2 are less intense than the similar structures in figure 1. They are less easily detected when viewing differences uncorrected for solar rotation or instantaneous images. The CME catalog indicates at 20:26 a 125°wide CME

around position angle 240°, counted from north in the positive direction. This possibly matches the direction from the feet of the brightened loops to the limb darkening.
In the case of figure 3 a dimming is observed from 14UT to 19UT, with no clear counterpart in the CME catalog.
In the case of figure 4 a weak dimming is observed at 171Å from 7UT to 13UT, with no event in the CME catalog between 01:30UT and O3:08 UT next day. This weak dimming is clearly undetected from differences uncorrected for solar rotation. It appears when closely inspecting instantaneous images at the location revealed by the corrected difference.

3 Studies of solar structures

3-1 halo CMEs

The april 7 1997 halo CME, Zarro et al. (1999), entered the field of view of the C2 coronograph at 14 :27. Five hours later the EIT synoptic differences between April, 7 and april, 6, figure 5, display clearly dimmings around the eruptive site.

On may 12, 1997 the measured positions of a halo CME are extrapolated back around 04:00 at the solar surface. The dimmings on the coronal synoptic differences between 01UT et 07UT, figure 6, are also clearly detected from inspection of the relevant instantaneous images. This is not the case for the nominally chromospheric HeII 304Å channel. Some minor artefacts, north-south stripes, appear on differences available at http://helios.izmiran.rssi.ru/lars/Chertok/Dimming/970512/4lines.jpg,

whereas using the latest calibration scheme we obtain, figure 6, a cleaner background.

The middle row of figure 7 is related to a halo event from the CME catalog. The dark area seen at 304Å westward from the erupting site is also clearly seen as a dark area in the 19UT instantaneous image. As no counterpart is available in the other channels this dimming could be attributed to some obscuring material, transparent at coronal wavelengths.

On May 1-2, 1998, the extrapolated origins of a series of three halo CMEs followed sharply by a stream of particles are respectively at 22:04, 03:55 and 13:07. As the uncertainty domain for the third time in this series covers the time slot devoted to the synoptic observations around 13:00 UT, this may explain the large differences between the second and the third row of figure 8.

By contrast, in the case of an isolated halo CME on June 6, 2000, followed gradually by particles, studied by Song, 2002, the extrapolated origin at the solar surface is around 15:11. This is clearly between the 13UT and 19UT times of the synoptic program. As a result the last bottom rows of figure 9 display similar features. The dimmings are strongest in the 284Å

coronal line of FeXIV. It is not clear whether the 304Åobservations are mainly related to the chromospheric HeII line or to the coronal SiXI line.

3-2 a wide CME

On February 28, 2001, a 232° wide CME towards 252°is clearly related to dimmings observed in a series of four frames by Yohkoh SXT from 12:54 to 13:24 (http://solar.physics.montana.edu/nuggets/2001/010316/sxt_fd.jpg). The EIT 284Å difference similarly reveals two darkenings inside the concavities of a S shaped curve, figure 10. Due to the 5" resolution of figure 10 we also note that at 13UT the filament centered on the sigmoid at 07UT has moved SW, i.e. in the direction of the CME. The cone-shaped darkening standing out in the 13UT-07UT 304Å synoptic difference is clearly absent from the quasi simultaneous 171Å and 284Å differences. The presence of a ghost brightening in the next difference indicates the transient nature of this darkening. We suggest this darkening is similar to the larger structure observed in figure 7.

3-4 an helical CME

An helical CME occurred on December 12, 1997 (Ciaravella et al., 2000). An erupting prominence appears at the NW limb on the 01UT 304Å synoptic image. It is not clear from this single image whether the feet of the preeruptive structure where located on the visible hemisphere or on the opposite hemisphere.We remark on the 284Å difference from 01UT to 19UT, in figure 11, that a part of the active region possibly connected to the prominence is missing. This fact is, in our opinion, not detectable by inspection of the instantaneous images. We suggest that the three events, helical CME, eruptive prominence and coronal dimming, are related.

3-5 prominence eruption

Figure l2 displays with six hours time interval the evolution of a filament in the northern hemisphere on April 18, 1999. In the first row, as a tribute to the quality of the correction for apparent rotation, the quiescent filament is not visible. In the second row the filament remains undetected in the 171Å and 284Å differences, whereas a slight motion is detected in the 304Å difference: this is the slow initiation of the disappearance studied by Sterling and Moore, 2004.

In the third row the filament is clearly detected, as well as dimmings in the 284Å difference. Inspecting the CME watch data reveals a disappearance in three steps: stability at 06:48, slight apparent displacement at 07:13, "disparition" at 07:36. Due to the fact that, in the absence of data from the STEREO mission, our observations are taken from a single point,

we cannot disentangle whether the filament is detected from a vertical or from an horizontal displacement. In addition to the post-eruptive arcades in the fourth row we note the presence of two circular dimmings, one on each side of the arcades. The visibility of these two dimmings is high, average and low respectively at 284Å, 171Å and 304Å.

3-6 prominence eruption whitout CME

We reproduce here a table from Choudary, 2004 with some additional information obtained from inspection of data from the EIT synoptic program difference atlas. The symbols – , + or * stand respectively for absent, faint or strong dimmings.

Date	*location*		*time*	*CME?*	*304Å*	*171Å*	*284Å*
February 26, 2000	*E50*	*N40*	*23 :26*	*Y*	-	-	-
March 4, 2000	*E50*	*S30*	*16 :24*	*Y*	+	-	+
September 12, 2000	*O40*	*S40*	*11 :21*	*Y*	+	-	+
November 24, 2002	*E50*	*N20*	*19 :43*	*Y*	+	+	+
January 3, 2003	*O90*	*N30*	*16 :25*	*Y*	-	-	-
January 14, 2003	*E90*	*S25*	*17 :25*	*Y*	+	-	-
March 13, 2003	*E50*	*N55*	*22 :19*	*Y*	+	-	-
March 14, 2003	*O50*	*S30*	*17 :15*	*Y*	+	-	-
May 1st, 2003	*E40*	*N30*	*15 :14*	*N*	*	*	*
May 2d, 2003	*O40*	*S20*	*18 :40*	*N*	*	-	*
June 9, 2003	*E50*	*N10*	*21 :00*	*N*	*	-	*
June 23, 2003	O60	S20	20 :33	Y	-	-	+

We note that in a series of twelve disappearing filaments the most intense dimmings are observed in the case where no CME follows. This somehow implies that these dimmings are not mainly due to the removal of emitting plasma, but possibly arise from temperature fluctuations.

3-7 gradual tether release of a filament

Although the usual observing wavelength for the CME watch program is 195Å, this was occasionally switched to 304Å, 171Å or 284Å. Sterling and Moore, 2003, studied at high cadence in the FeXIV 284Å line the slow release of a prominence from 16UT, February 8, 1999 until 02UT next day. The synoptic program differences, figure 13, display some dimming at 304Å, 195Å and 284Å. This may be attributed to the removal of high temperature plasma if we consider that the 304Å signal is mainly due to the SiXI line. By contrast the different relative amplitude of dimmings available in figure 14 is attributed to the removal of lower temperature plasma.

4 Summary and Conclusion

On account of three incentively propitious properties of the EIT synoptic data set: the length of its time interval around the maximum of the 23d solar cycle, the full solar disk size of its

field of view, and the large temperature range of its four wavelengths, we built an atlas of solar events, despite an unsatisfactorily coarse time sampling of a six hour cadence.

From a subset of fourteen observations, corrected from the parasitic effect of the solar rotation, we foretaste the anticipated results of future solar missions. On one side, different wavelength dependent responses indicate temperature variations of the solar plasma; on the other side similar responses may help in order to estimate the mass flux of CMEs.

5 References

Brueckner, G.E., Howard, R.A., Koomen M.J. et al. The large angle spectroscopic coronograph (LASCO) Visible light coronal Imaging and spectroscopy, Solar Physics162 :357-402, 1995.

Ciaravella, A., Raymond, J., Thompson B . et al Solar and Heliospheric Observatory observations of a helical coronal mass ejection, Astrophys. J. 529 : 575-591, 2000.

Chertok, I. and Grechnev, V solar large-scale channeled dimmings produced by coronal mass ejections, Astronomy Reports vol. 47 n°2, pp. 139-150, 2003.

Choudary, D. and et Moore, R. filament eruption without coronal mass ejection Geophysical Research Letters vol. 30 n°21 : 2107,SSC7-1 :7-4, 2004.

Delaboudinière, J.P., _Artzner , G., Brunaud, J. et al. EIT: Extreme-ultraviolet Imaging Telescope for the SOHO mission Solar Physics vol. 162 pp. 291-312, 1995.

Domingo, V., Fleck, B., and Poland, A.I., and A.I. The SOHO Mission: An Overview, Solar Physics 162, pp 1-37, 1995.

Song, L., Zhang, J., Yang, Z. and Wang, J . atmospheric dynamics and magnetic activity associated with a coronal mass ejection Solar Physics 211 : 315-331, 2002.

Sterling, A. and Moore, R. tether-cutting energetics of a solar quiet-region prominence eruption Astrophys. J**.** 599 : 1418-1425, 2003.

Sterling, A. and Moore, R. evidence for gradual external reconnection before explosive eruption of a solar filament, Astrophys. J**.** 602 : 1024-1036, 2004.

Zarro, D., Sterling, A., Thompson, B. et al. SOHO EIT observations of extreme-ultraviolet "dimming" associated with a halo coronal mass ejection, Astrophys. J. 520 : L139-L142, 1999.

ftp://ftp.ias.u-psud.fr/pub/gartzner/GEA/biblio_differences-EIT.htm

http://helios.izmiran.rssi.ru/lars/Chertok/Dimming/970512/4lines.jpg

http://cdaw.gsfc.nasa.gov/CME_list/

http://solar.physics.montana.edu/nuggets/2001/010316/sxt_fd.jpg

6 Acknowledgments

The CME catalog is generated and maintained by NASA and The Catholic University of America in cooperation with the Naval Research Laboratory.

SOHO is a project of international cooperation between ESA and NASA

7 Figure Captions

Italic script numbers pertain to the number in our catalog of synoptic differences for the first difference image in the current figure.

figure1(*23729*) october 25, 2001.

304Å	171Å	284Å
07 :19-01 :19	07 :00-01 :00	07 :05-01 :05
13 :19-07 :19	13 :00-07 :00	13 :05-07 :05
19 :19-13 :19	19 :00-13:00	19 :05-13 :05

1091km/s halo CME entering C2 field of view at 15:26, origin extrapolated at 14:50 UT

.

figure 2 (*26805*) may 19 – 20, 2002.

304Å	171Å	284Å
13 :19-07 :19	13 :00-07 :00	13 :05-07 :05
19 :19-13 :19	19 :00-13 :00	19 :05-07 :05
01 :19-19 :19	01 :00-19 :00	01 :06-19 :05

541km/s 125° wide CME towards 226° entering C2 field of view at 15:26, origin extrapolated shortly before 20UT

Figure 3 (*6109*) February 1st, 1998.

304Å	171Å	284Å
08 :29 –01 :58	08 :11-01 :40	08 :16-01 :45
14 :40-08 :29	14 :21-08 :11	14 :27 –08 :16
19 :31-14 :40	19 :13-14 :21	19 :19-14 :27

270km/s 63° wide CME towards 78° entering C2 field of view at 20:27, origin extrapolated 17:30 UT
450km/s 30° wide CME towards 244° entering C2 field of view at 22:37, origin extrapolated ---21:30UT

Figure 4 (*6245*) February 10, 1998.

304Å	171Å	284Å
01 :20 –19 :19 february, 9	01 :00-19 :00	01 :06-19 :05
07 :20-01 :20	07 :00-01 :00	07 :06 –01 :06
13 :20-07 :20	13 :00-07 :00	13 :06-01 :06

no CME between February 10, 01:30 and february 11, 03:08

Figure 5 (*2085*) halo CME april 7, 1997.

304Å	171Å	284Å
april 6,1997 19 :59 -april 5, 22 :08	19 :53-22 :02	19 :46-21 :55
april 7, 1997 19 :42- april 6, 19 :59	19 :29-19 :53	19 :35-19 :46

818 km/s halo CME entering C2 field of view at 14:27, origin extrapolated 13:50 UT

Figure 6 (*2557*) may 12, 1997

304Å	171Å	284Å
01 :18 –19 :18 may 11	01 :00-19 :00	01 :06-19 :06
07 :18-01 :18	07 :00-01 :00	07 :06 –01 :06
13 :18-07 :18	13 :00-07 :00	13 :06-01 :06

464 km/s halo CME entering C2 field of view at 05:30, origin extrapolated 03:50UT

Figure 7 (*7341*) april 29, 1998.

304Å	171Å	284Å
13 :25 –19 :22 april 29	13 :06-19 :02	13 :11-19 :08
19 :24-13 :25	19 :04-13 :26	19 :10 –13 :11

1374 km/s halo CME entering C2 field of view at 16:58, origin extrapolated at 16:20 UT

Figure 8 (*7385*) may 2, 1998.

304Å	171Å	284Å
07 :24-01 :24	07 :04-01 :04	07 :10-01 :10
13 :27-07 :24	13 :07-07 :04	13 :13-07 :10
18 :30-13 :27	18 :10-13 :07	18 :16-13 :13

938 km/s halo CME entering C2 field of view at 14:06, origin extrapolated at 13:10 UT

Figure 9 (*16293*) june 6, 2000.

304Å	171Å	284Å
01 :19 –19 :19	01 :00-19 :00	01 :06-19 :06
07 :19-01 :19	07 :00-01 :00	07 :06–01 :06
13 :19-07 :19	13 :00-07 :00	13 :06-07 :06
19 :19-13 :19	19 :00-13 :00	19 :06-13 :06

1119 km/s halo CME entering C2 field of view at 15:54, origin extrapolated at 15:10 UT

Figure 10 (*20289*) February 28, 2001.

304Å	171Å	284Å
07 :19-01 :19	07 :00-01 :00	07 :06–01 :06
13 :19-07 :19	13 :00-07 :00	13 :06-07 :06
19 :19-13 :19	19 :00-13 :00	19 :06-13 :06
01 :19-19 :19	01 :00-19 :00	01 :06-19 :06

313 km/s 232° wide CME towards 252° entering C2 field of view at 14:50, origin extrapolated at 13:23 UT

Figure 11 (*5432*) december 11 and December 12, 1997

284Å.

13 :05-07 :05
19 :07-13 :05
01 :05-19 :07
07 :05-01 :05

231 km/s 34° wide CME towards 46° entering C2 field of view at 19:57, origin extrapolated at 16:30 UT
211 km/s 80° wide CME towards 291° entering C2 field of view at 01:27, origin extrapolated at 22:35 UT

Figure 12 (*10141*) april 17 and april 18, 1999.

304Å	171Å	284Å
19 :19-13 :19	19 :00-13 :00	19 :06-13 :06
01 :19-19 :19	01 :00-19 :00	01 :06-19 :06
07 :19-01 :19	07 :00-01 :00	07 :06–01 :06
13 :19-07 :19	13 :00-07 :00	13 :06-07 :06

475 km/s 112° wide CME towards 59° entering C2 field of view at 08:30, origin extrapolated at 07:30 UT

Figure 13 (*9173*) February 8 and February 9, 1999.

304Å	171Å	195Å	284Å
19 :22-13 :22	19 :03-13 :03	19:16-13:16	19 :09-13 :09
01 :22-19 :22	01 :03-19 :03	01:16-19:16	01 :09-19 :09

853 km/s 60° wide CME towards 47° entering C2 field of view at 01:30, origin extrapolated at 01:03 UT

Figure 14 (*9177*) February 9, 1999.

304Å	171Å	195Å	284Å
01 :22-19 :22	01 :03-19 :03	01:16-19:16	01 :09-19 :09
07 :22-01 :22	07 :03-01 :03	07:16-01:16	07 :09-01 :09

808 km/s 132° wide CME towards 238° entering C2 field of view at 05:33, origin extrapolated at 04:50 UT

Figure

Click here to download high resolution image

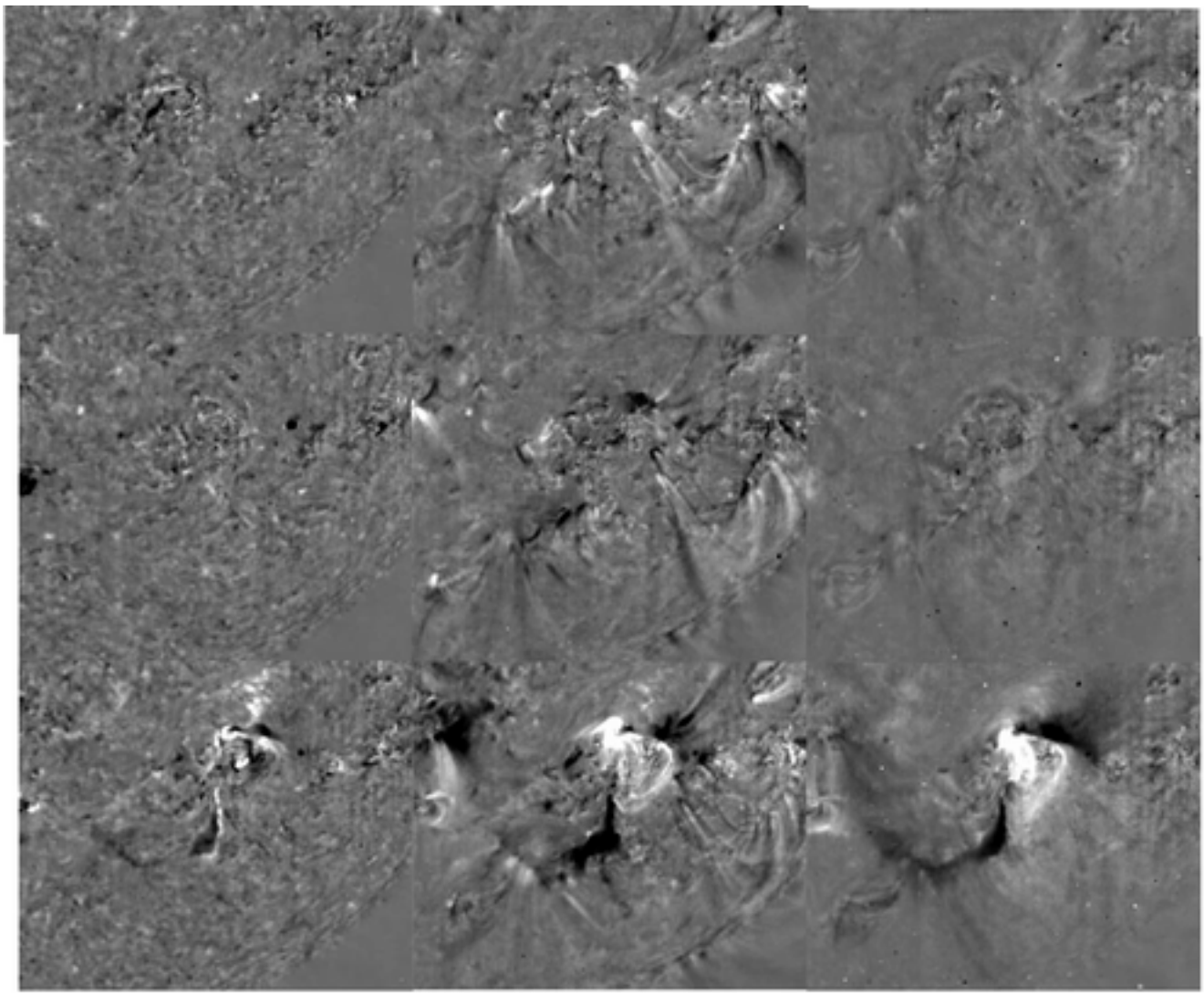

Figure

Click here to download high resolution image

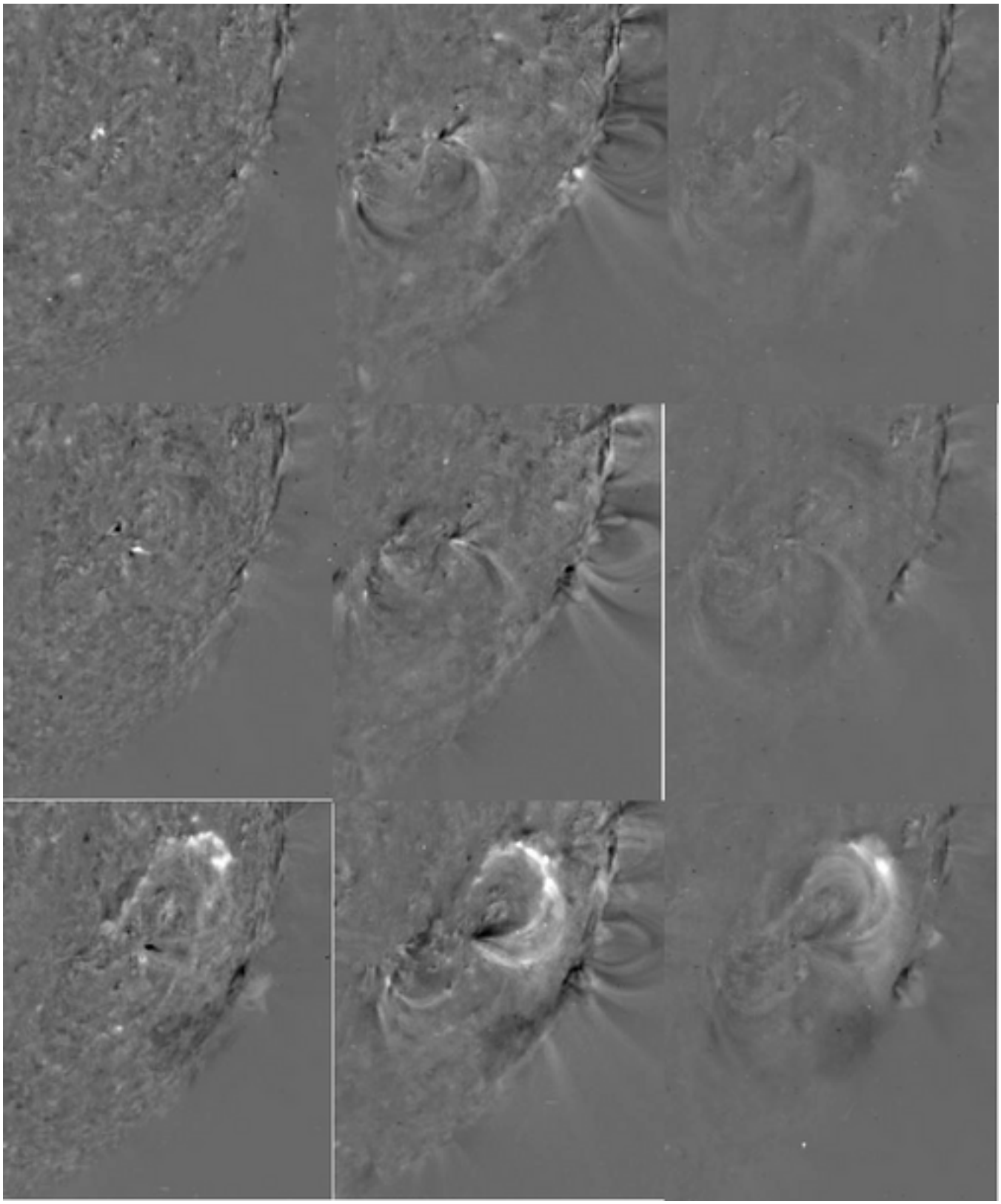

Figure

Click here to download high resolution image

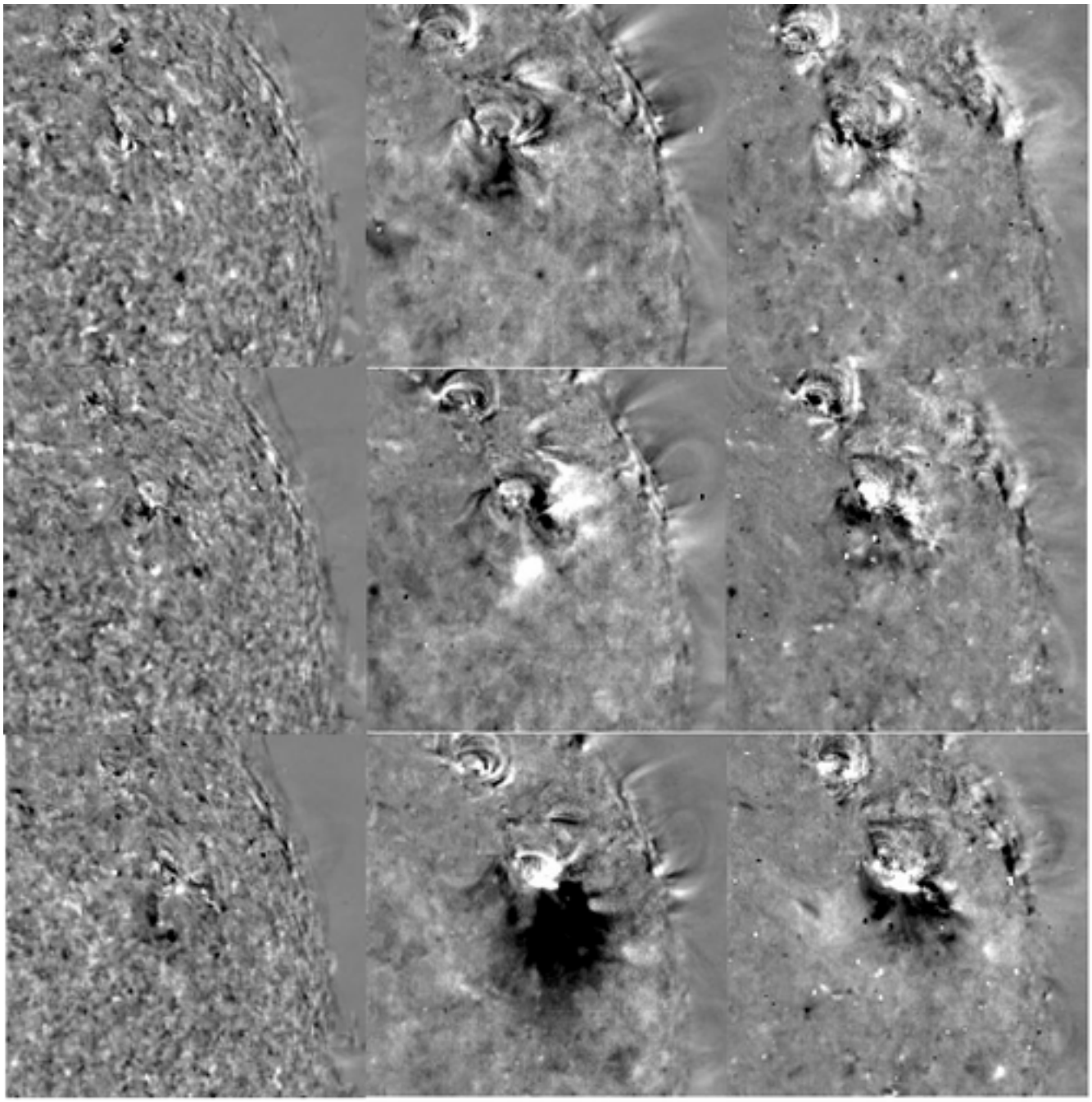

Figure

Click here to download high resolution image

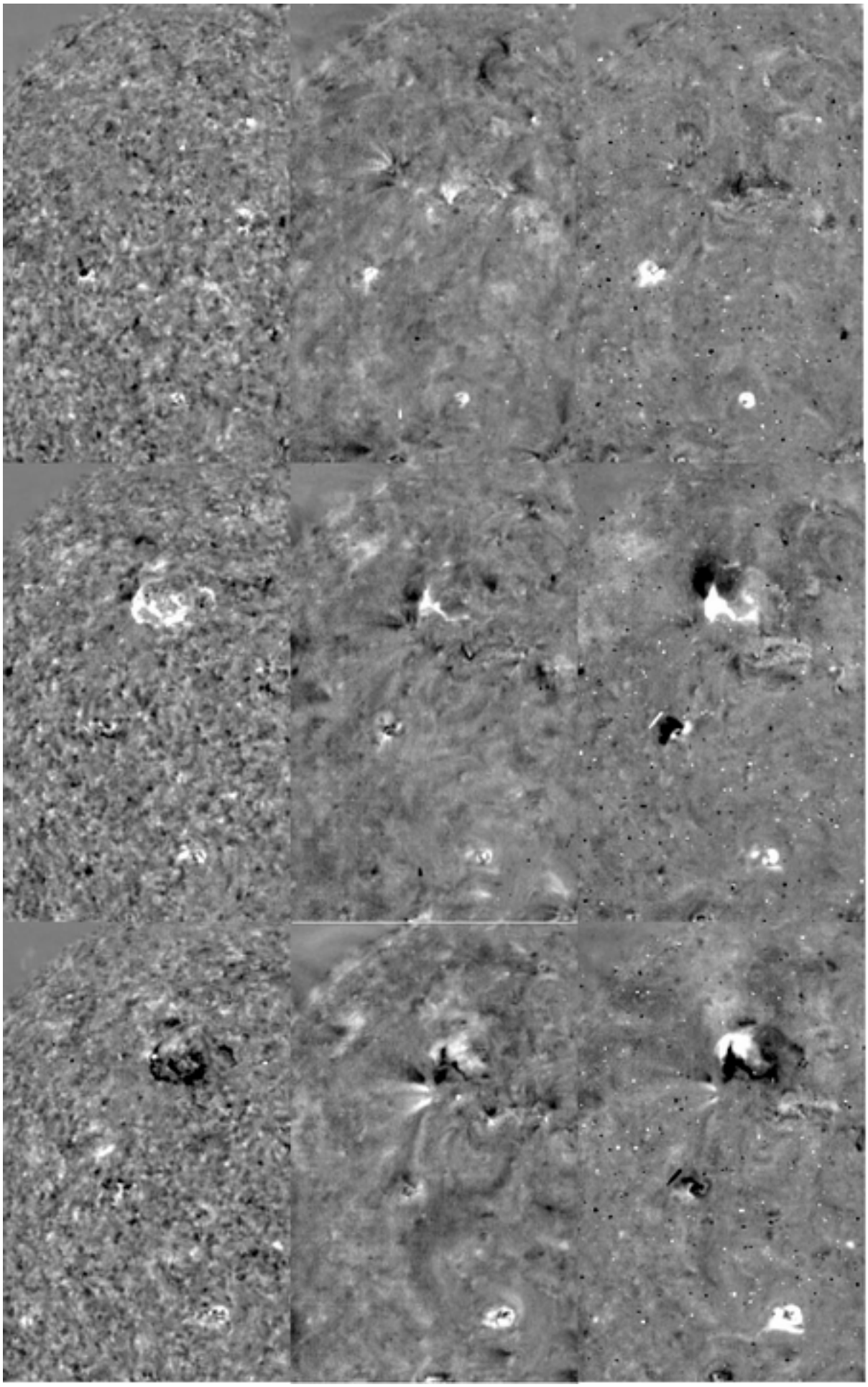

Figure

Click here to download high resolution image

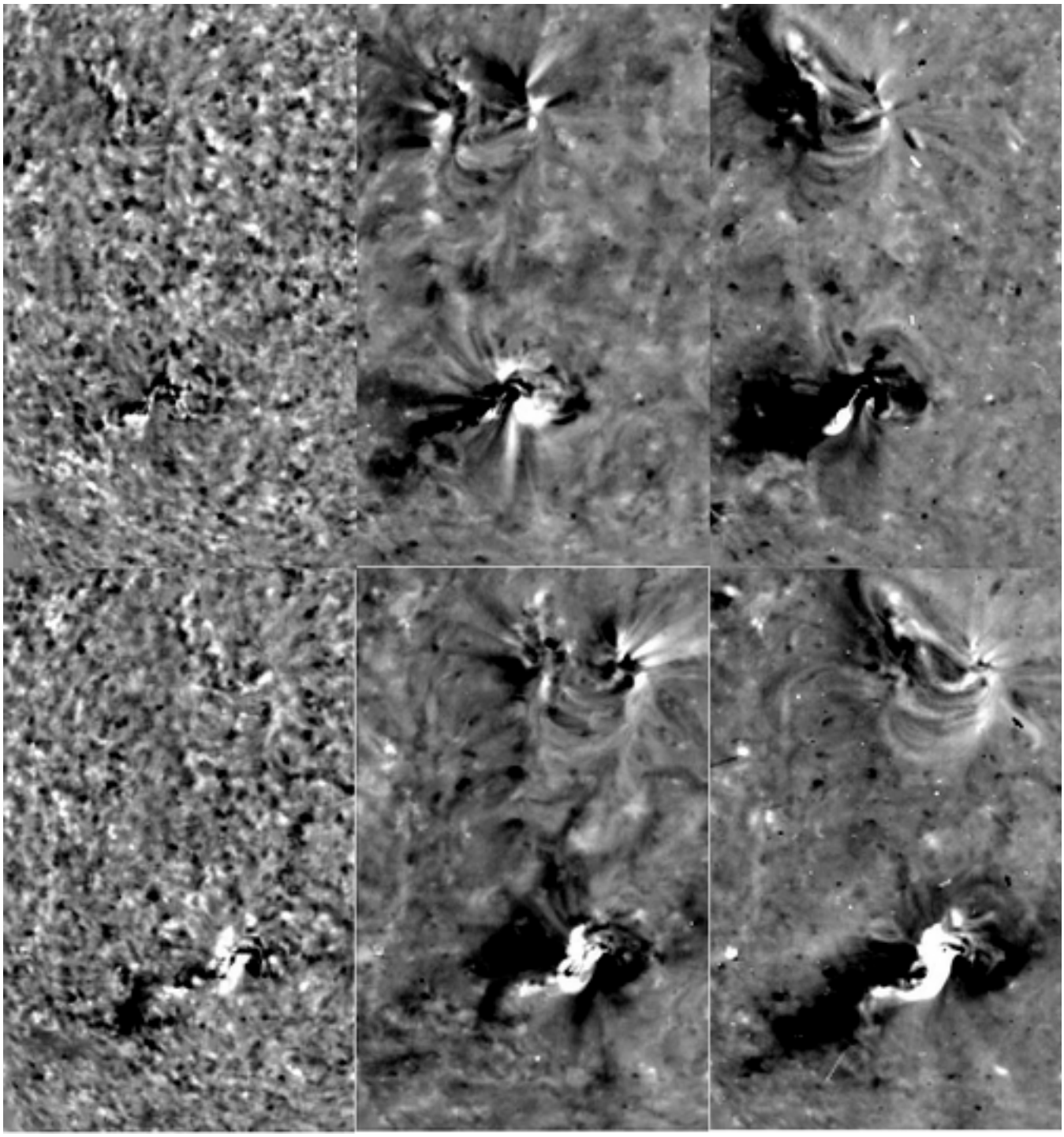

Figure

Click here to download high resolution image

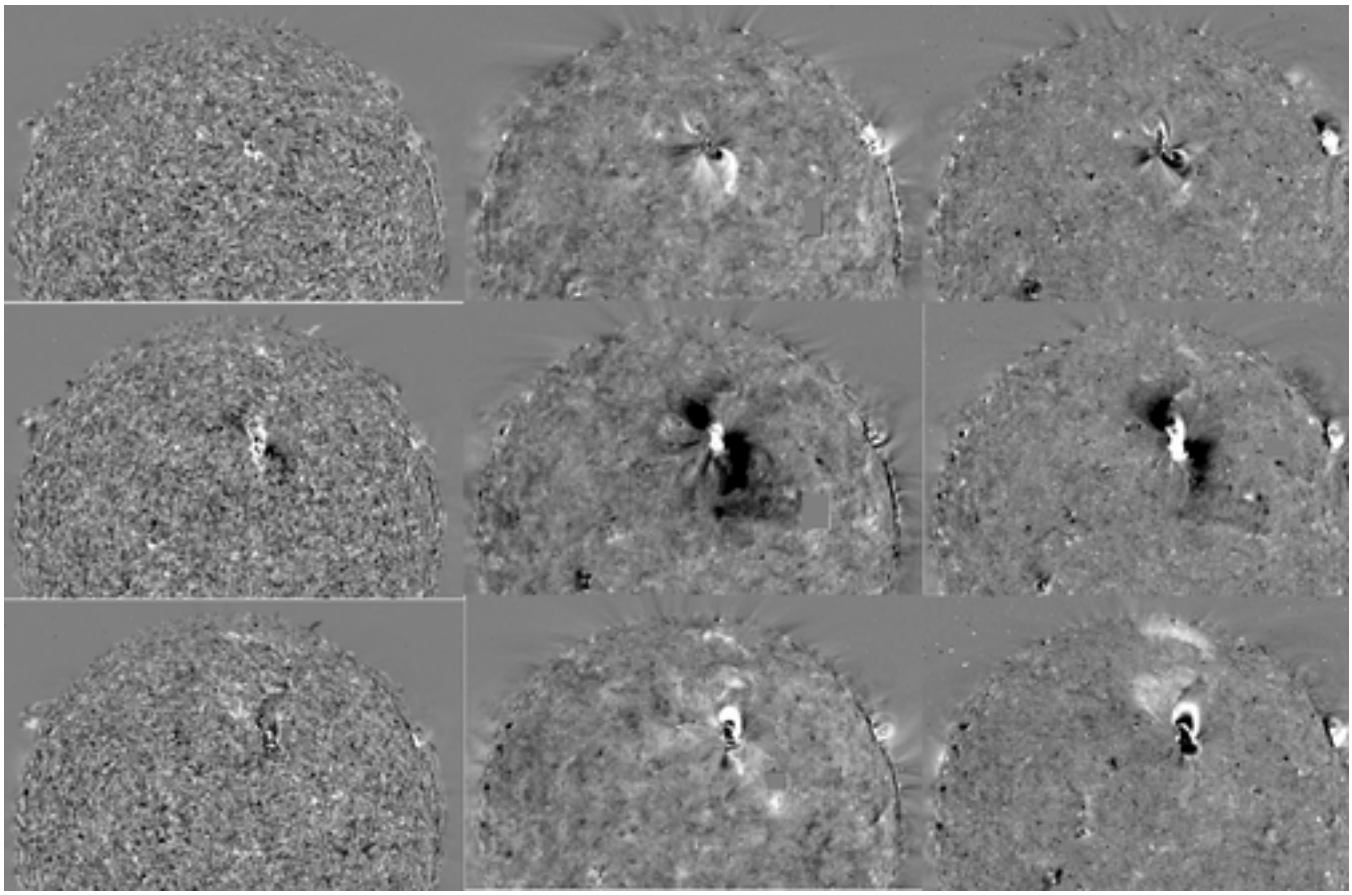

Figure

Click here to download high resolution image

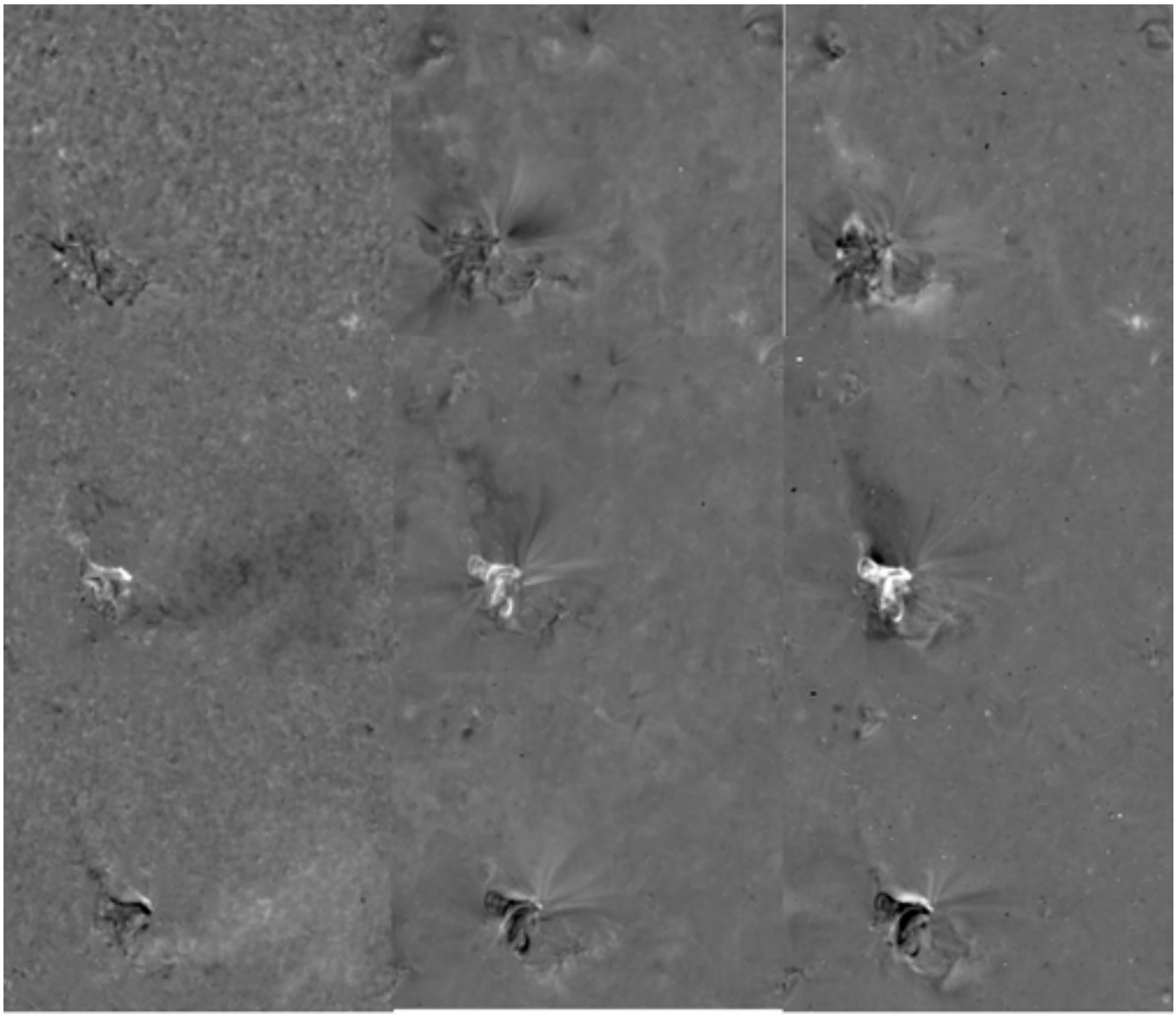

Figure

Click here to download high resolution image

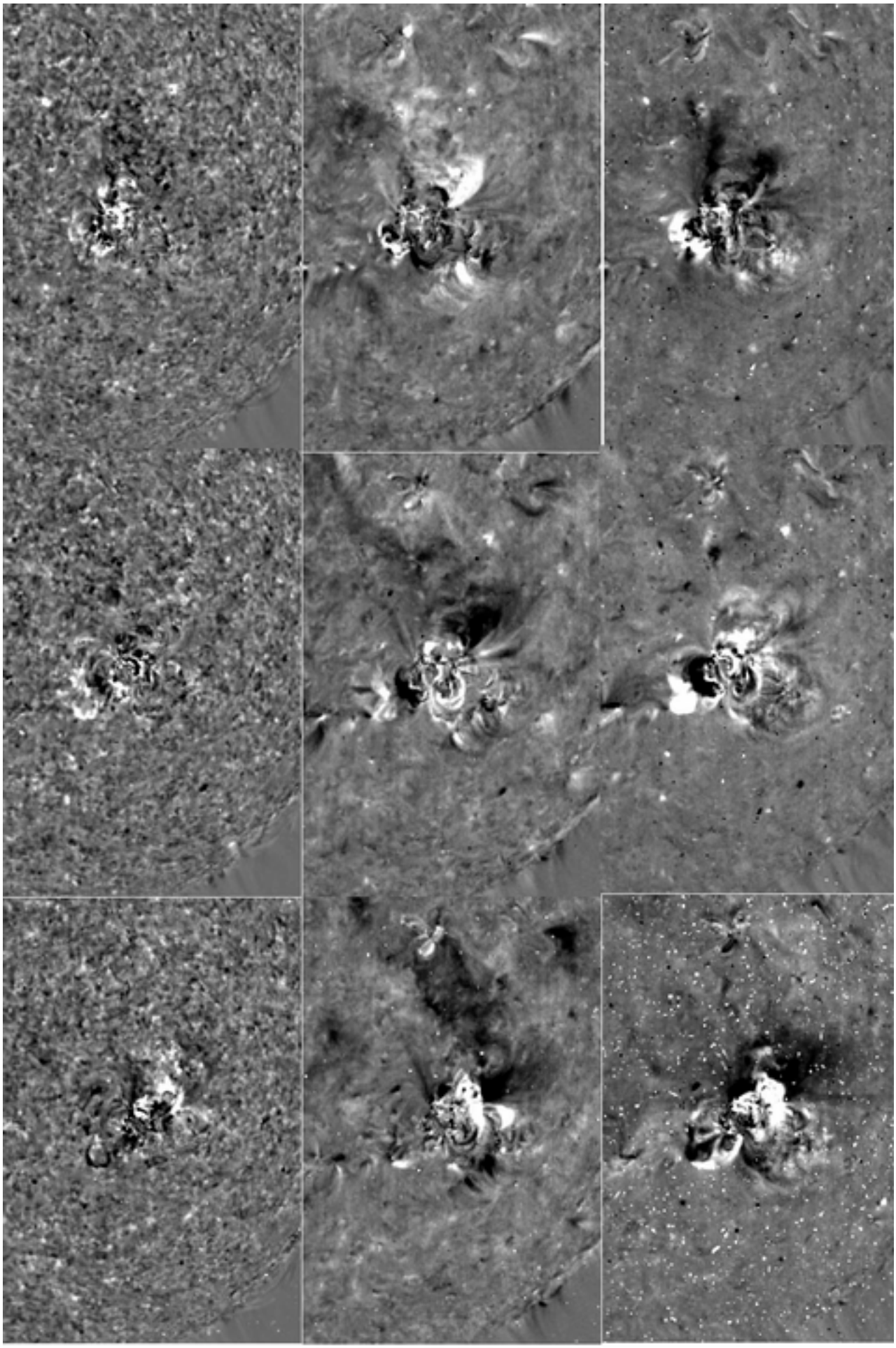

Figure

Click here to download high resolution image

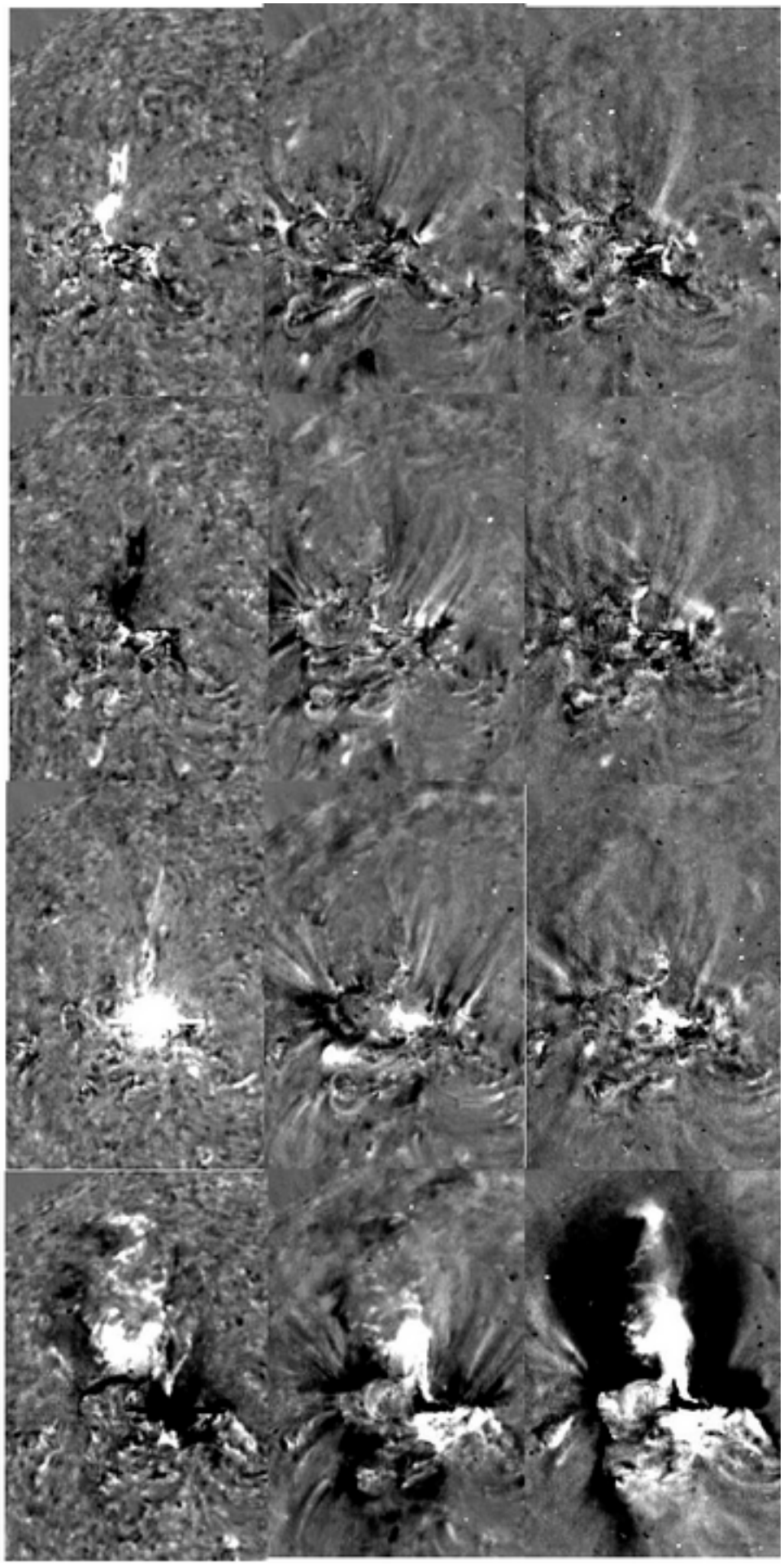

Figure

Click here to download high resolution image

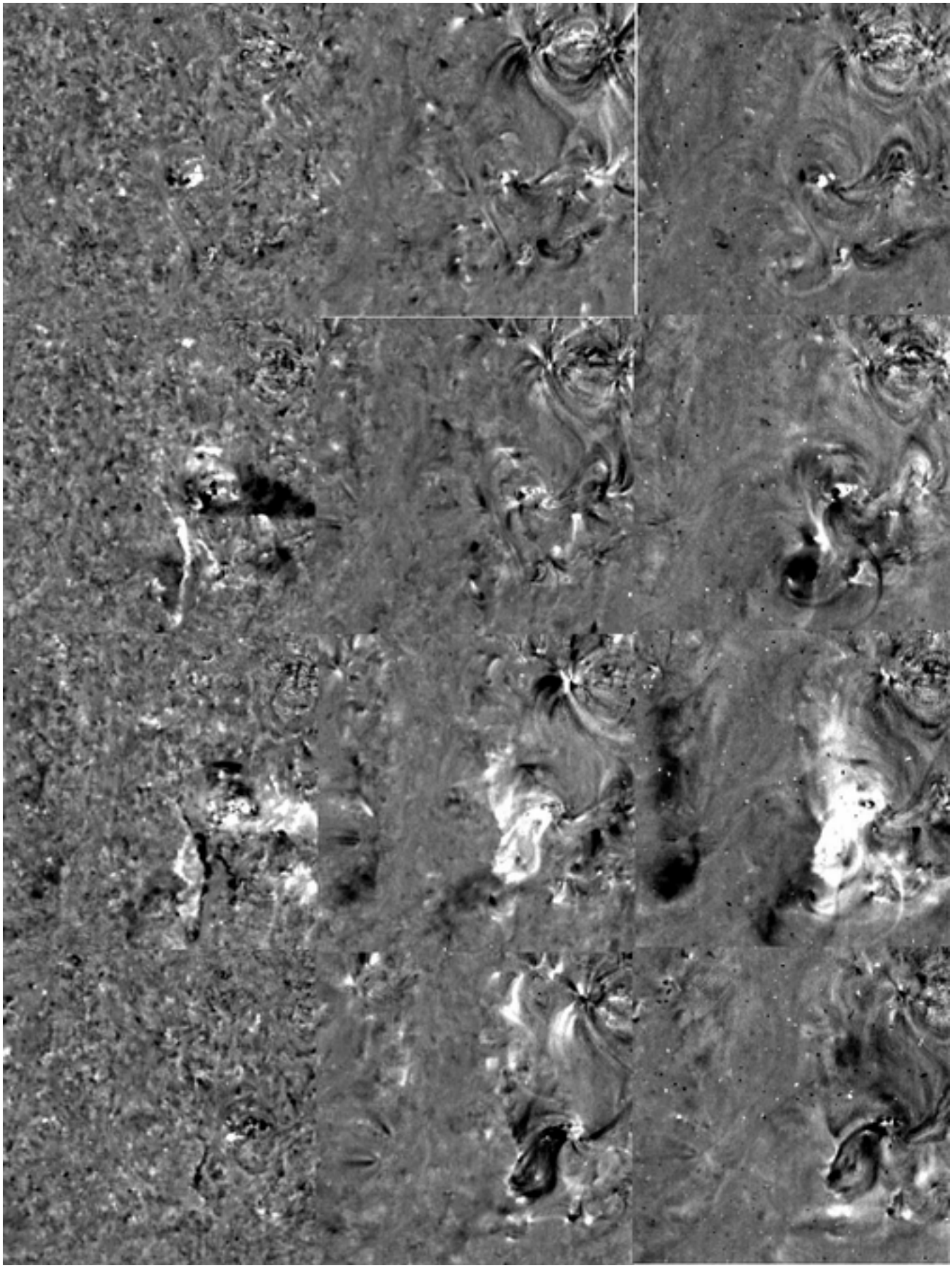

Figure

Click here to download high resolution image

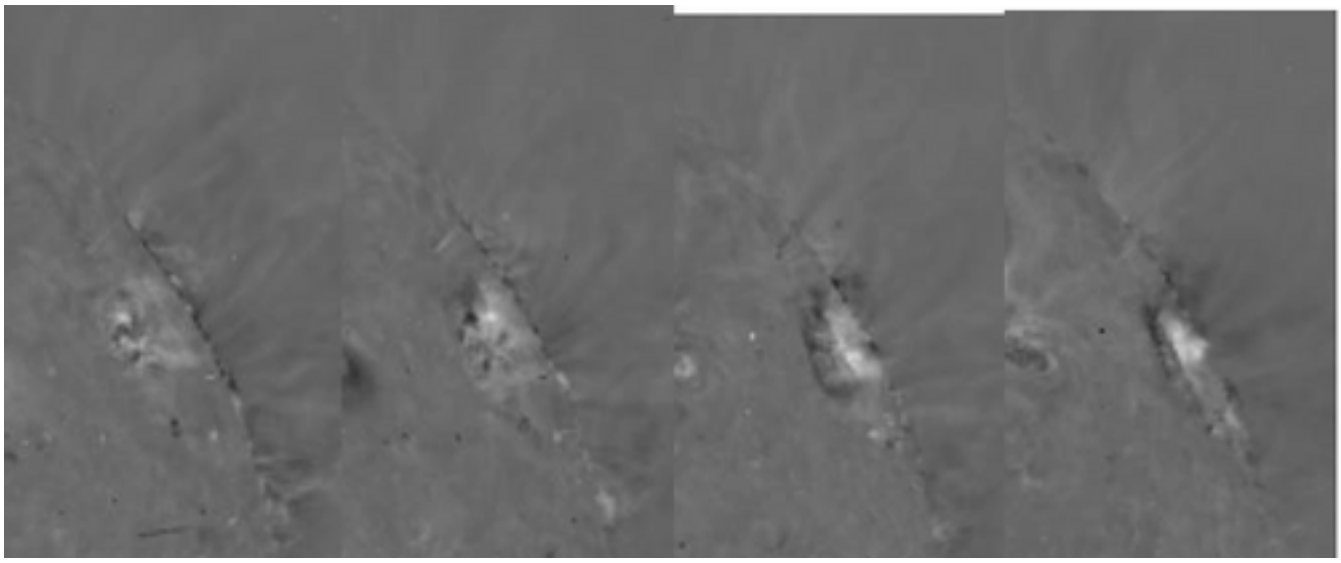

Figure

Click here to download high resolution image

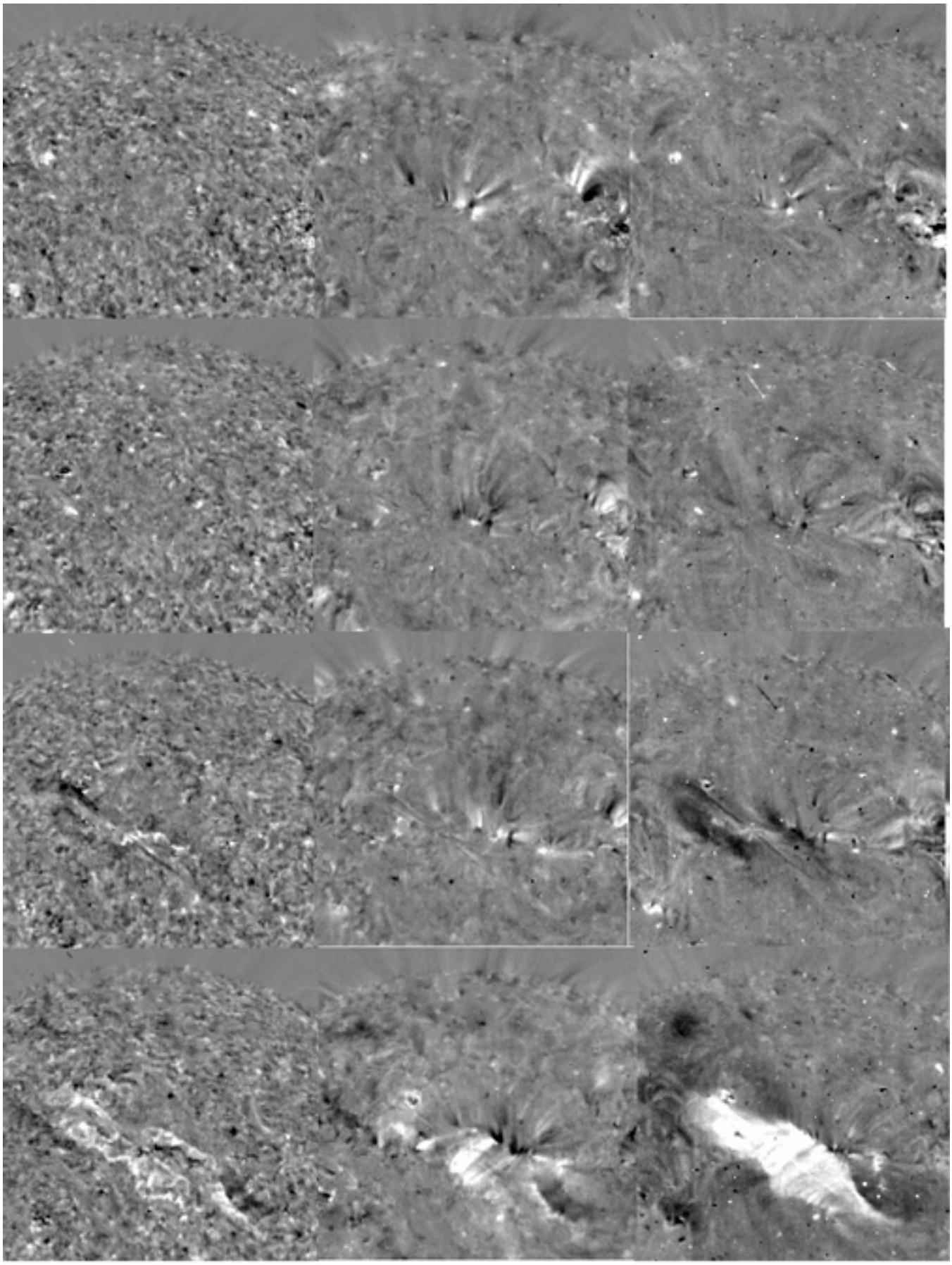

Figure

Click here to download high resolution image

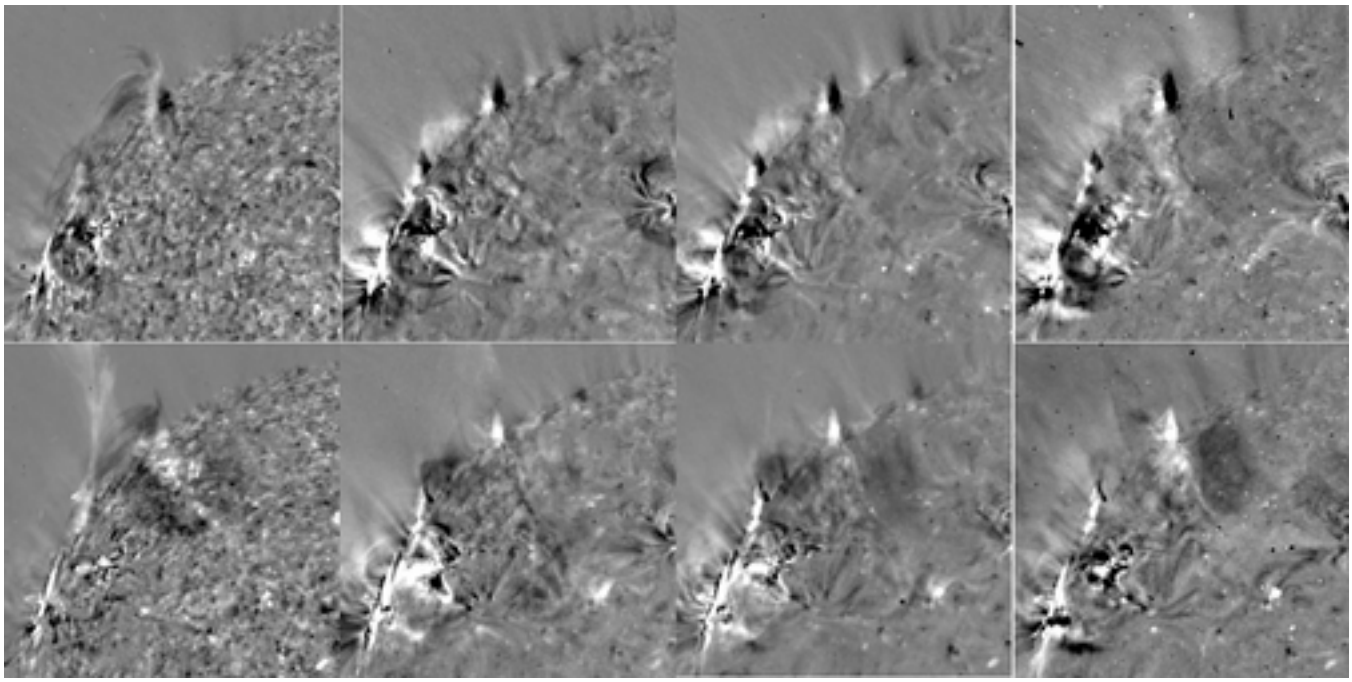

Figure

Click here to download high resolution image